ARTICLE

Direct Writing of Sub-5 nm Hafnium Diboride Metallic Nanostructures

Wei Ye,[†,‡,*] Pamela A. Peña Martin,[‡] Navneet Kumar,[‡] Scott R. Daly,[⊥] Angus A. Rockett,[‡] John R. Abelson,[‡] Gregory S. Girolami,[⊥] and Joseph W. Lyding[†,‡,§]

[†]Beckman Institute for Advanced Science and Technology, [‡]Department of Materials Science and Engineering, [§]Department of Electrical and Computer Engineering, and [⊥]School of Chemical Sciences, University of Illinois at Urbana—Champaign, Urbana, Illinois 61801

ABSTRACT Sub-5 nm metallic hafnium diboride (HfB_2) nanostructures were directly written onto Si(100)-2 × 1:H surfaces using ultrahigh vacuum scanning tunneling microscope (UHV-STM) electron beam induced deposition (EBID) of a carbon-free precursor molecule, tetrakis(tetrahydroborato)hafnium, $Hf(BH_4)_4$. Scanning tunneling spectroscopy data confirm the metallic nature of the HfB_2 nanostructures, which have been written down to lateral dimensions of ~2.5 nm. To our knowledge, this is the first demonstration of sub-5 nm metallic nanostructures in an STM-EBID experiment.

KEYWORDS: scanning tunneling microscopy · electron beam induced deposition · hafnium diboride · scanning tunneling spectroscopy · nanowire · nanodot · sub-5 nm

The patterning of metallic nanostructures on surfaces is of great interest in fabricating nanoelectronics and quantum devices. For example, nanometer scale metals are potentially useful not only as interconnects between devices but also as functional elements of Coulomb blockade devices such as single electron transistors (SETs).[1] To operate a SET at room temperature, the island size must be smaller than 10 nm.[2] Current top-down fabrication technologies used in industry involve conventional lithographic processes, which are approaching their fundamental size limits. Sub-10 nm features are hard to achieve using the conventional lithographic technology, even for electron beam lithography.[3] To overcome this barrier, new fabrication strategies must be developed.

In 1994, Lyding *et al.* demonstrated creating atomic scale silicon dangling bond patterns on a hydrogen-passivated Si(100)-2 × 1 surface using a UHV-STM.[4] The difference in reactivity between bare and hydrogen-terminated silicon allows nanometer scale metal patterning on silicon surfaces.[5] Both physical vapor deposition (PVD)[6−14] and chemical vapor deposition (CVD)[15−19] methods were exploited for metal delivery to silicon substrates. In most PVD experiments, metal grows preferentially on bare silicon areas. However, undesired metal growth on the hydrogen-terminated region limits its application. In contrast, a molecular precursor dissociates and deposits metal primarily on the bare silicon area by CVD, leading to minimal contamination of the hydrogen-terminated background. In CVD, the substrate is usually heated to induce the CVD reaction. The precursor molecules must be carefully chosen so that the CVD reaction temperature will not exceed the hydrogen desorption temperature (520 °C).[20]

Electron beam induced deposition (EBID) is an alternative to the PVD and CVD methods. It is a direct writing method which forgoes the nanolithography steps and no substrate heating is required.[21] EBID employs a scanning electron microscope electron beam to crack molecules that are introduced to a surface in the gas phase. Typically, these molecules are the same ones used for thermal CVD. To further enhance the spatial resolution of EBID, a negatively biased scanning tunneling microscope (STM) tip can be used as the electron source. The resulting fragments deposit onto the surface in patterns governed by the movement of the STM tip. STM-EBID experiments have been performed to write sub-10 nm features using CVD precursors for several metals, including W,[22] Fe,[23,24] Al,[18,25] Ti,[16] Ni,[26] and Pd,[27] but these experiments did not confirm that the deposits were metallic, for example, by means of transport or scanning tunneling spectroscopy (STS) measurements. Most CVD precursors afford pure films only if certain specific bonds are cleaved; in contrast, primary electrons from the EBID beam and secondary electrons emitted by the surface are en-

*Address correspondence to weiye@illinois.edu.

Received for review July 31, 2010 and accepted October 18, 2010.

Published online October 22, 2010. 10.1021/nn1018522

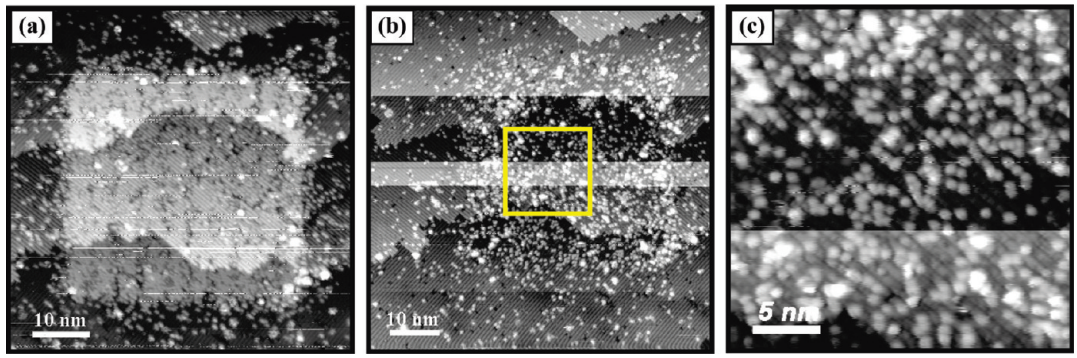

Figure 1. (a) Filled states STM image after desorbing hydrogen in a square pattern by writing closely spaced parallel lines at a sample bias of 7 V, 0.1 nA and a line dose of 1.0×10^{-4} C/cm. (b) STM image of the patterned Si(100)-2 × 1:H surface after dosing with $Hf(BH_4)_4$ at room temperature. (c) Enlarged image of area highlighted in (b).

ergetic enough to break every bond. For this reason, EBID often is unable to produce the clean deposits that are characteristic of CVD with the same precursor. For example, EBID of organometallic CVD precursors typically results in the incorporation of high levels of carbon: whereas $Fe(CO)_5$ gives iron films under CVD conditions, STM-EBID deposition from this same precursor affords carbide films with carbon contents of 27−52 atom %.[23]

To avoid the carbon contamination issue while retaining the resolution benefits of STM-EBID, we have deposited metallic hafnium diboride (HfB_2) from a carbon-free precursor tetrakis(tetrahydroborato)hafnium, $Hf(BH_4)_4$. HfB_2 is a metallic ceramic with attractive engineering properties: a high melting point of 3250 °C, a low bulk resistivity of 15 $\mu\Omega \cdot$ cm, and a high bulk hardness of 29 GPa.[28] Recent research has shown that highly conductive HfB_2 thin films can be deposited by thermal CVD from $Hf(BH_4)_4$ at low CVD growth temperatures (≥200 °C).[29,30] In this work, we use the $Hf(BH_4)_4$ precursor to write metallic HfB_2 nanostructures directly onto hydrogen-passivated Si(100)-2 × 1 surfaces using STM-EBID at room temperature. Spatially resolved tunneling current−voltage ($I-V$) spectroscopy is used to characterize the electronic properties of the nanostructures.

RESULTS AND DISCUSSION

To investigate the adsorption of $Hf(BH_4)_4$ on the silicon surface and the selectivity of $Hf(BH_4)_4$ between bare and hydrogen-terminated silicon at room temperature, we patterned the Si(100)-2 × 1:H surface by desorbing hydrogen in selective areas. Figure 1a shows an image where the hydrogen has been desorbed in a square pattern by moving the STM tip in a series of closely spaced parallel lines. The sample patterning bias was 7 V, and the current and electron dose were 0.1 nA and 1.0×10^{-4} C/cm, respectively. The clean silicon appears brighter (~1.5 Å´ higher) in Figure 1a due to the enhanced density of states of dangling bonds.

Figure 1b shows the same patterned area after dosing $Hf(BH_4)_4$ at a local pressure of 2×10^{-6} Torr for 2 min at room temperature. The $Hf(BH_4)_4$ shows great selectivity between bare and H-terminated silicon. No adsorption of $Hf(BH_4)_4$ was observed on the hydrogen-terminated area, and even the silicon dangling bonds remained intact. However, more than 70% of patterned bare silicon area was repassivated. Further dosing of $Hf(BH_4)_4$ results in no change of the pattern. Figure 1c is a zoom-in image of the square area in Figure 1b taken from the interior of the patterned area. Silicon dimer rows are clearly visible all over the image; the bright ball-shaped features are unpassivated dangling bonds with a height around 1.5 Å´, while the repassivated regions are darker due to the lower density of states for tunneling.

Although the detailed mechanism of how the $Hf(BH_4)_4$ reacts with bare silicon surface is still under investigation, we speculate that at room temperature $Hf(BH_4)_4$ cracks dissociatively on Si(100). The atomic hydrogen produced in the process passivates the clean silicon surface. With the increase of the repassivated area, the decomposition of additional $Hf(BH_4)_4$ is inhibited due to a steric effect, leading to a partial repassivation.

It is important to note that no deposition of HfB_2 is observed on either the hydrogen-passivated or clean silicon areas. This is expected since the CVD reaction of $Hf(BH_4)_4$ will not occur under 200 °C.[29] We did not observe any adsorbed fragments on the surface after exposure to the precursor, suggesting a low sticking coefficient of Hf-containing species on both H-terminated and bare silicon surface. All features higher than dangling bonds observed in Figure 1c were present prior to exposure.

The aforementioned control experiment suggests that a certain amount of energy is required to initiate the HfB_2 deposition on the silicon surface. In contrast to conventional thermal CVD, which uses the thermal energy from the surface of a heated substrate, we use the electron beam from the STM tip to decompose the $Hf(BH_4)_4$ molecules and initiate the deposition under the tip. By repeatedly scanning the STM tip along a line path, well-defined HfB_2 nanowires are directly written

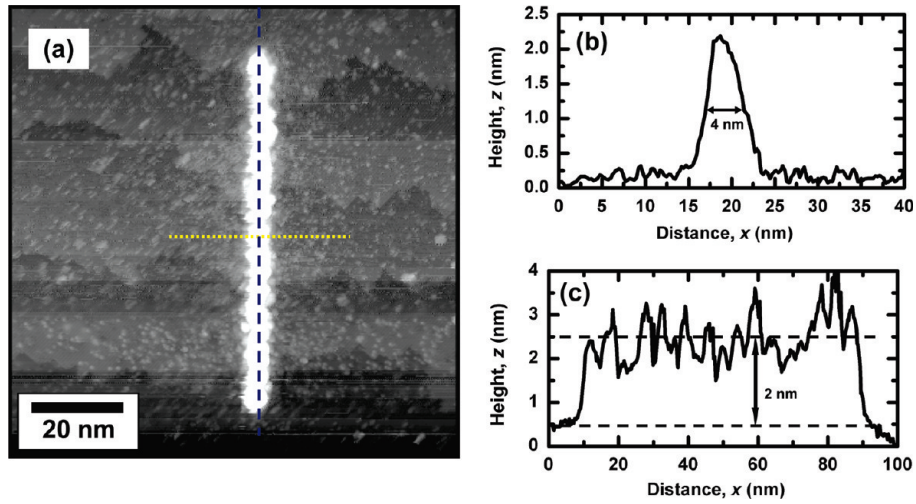

Figure 2. HfB_2 nanowires made by STM-EBID on a Si(100)-2 × 1:H surface. (a) A 100 × 100 nm^2 STM image after direct writing a HfB_2 line. Deposition conditions: sample bias = 7 V, I = 0.1 nA, $Hf(BH_4)_4$ pressure = ~1 × 10^{-5} Torr. (b) Line contour from (a) perpendicular to the nanowire (yellow dotted line). (c) Line contour from (a) parallel to the nanowire (blue dashed line).

onto the silicon surface. No deposit forms in the absence of the precursor, which rules out the possibility that the deposits are tungsten transferred from the tip. Figure 2a is a topographic image of a HfB_2 nanowire deposited on the surface using +7 V sample bias and 0.1 nA tunneling current. During deposition, the STM tip was scanned over a line 36 times with a writing speed of 10 nm/s. The $Hf(BH_4)_4$ background pressure is 5 × 10^{-9} Torr, which gives a local pressure of ~1 × 10^{-5} Torr. The height profiles in Figure 2b,c show that the resulting nanowires are only 4 nm wide and 2 nm thick on average. The HfB_2 is deposited only under the STM tip; the surrounding substrate remains clean. Deposition occurs at both positive and negative sample bias, with a much higher deposition rate at positive sample bias. By comparing the volume of the nanostructures fabricated at the same conditions except bias polarity, we found the deposition rate at positive sample bias could be 30 times greater than that at negative sample bias. The deposition rates increase with writing voltage, and no voltage threshold was observed so far. It is interesting to note that tip length increases at negative writing voltage, indicating HfB_2 grows on the tip. It could be used as a tip-conditioning method. In thermal CVD using the same precursor, Kumar *et al.* found that dehydrogenation of a hydrogen-terminated Si(100) substrate by remote plasma treatment enhanced the HfB_2 nucleation density by 2 orders of magnitude.[31] As a working hypothesis, we assume that hydrogen desorption by the STM tip is required before HfB_2 can grow in our experiment.

To investigate the mechanism by which the HfB_2 wires are deposited by STM-CVD, we wrote a series of wires with varying writing time. Figure 3a shows four HfB_2 nanowires deposited onto the Si(100)-2 × 1:H surface, varying only the number of repetitions. Wires 1−4 were deposited at a +5 V sample bias and a 1 nA tunneling current with a writing speed of 10 nm/s. The number of repetitions of each wire is 20, 40, 60, and 80 times, respectively, giving rise to a deposit time of 80, 160, 240, and 320 s, respectively, on each wire. The local $Hf(BH_4)_4$ pressure was ~4 × 10^{-6} Torr. Figure 3b shows a line contour taken from the topographic image in Figure 3a. The height of the HfB_2 nanowires increases with writing time, whereas the line width remains nearly the same. This result suggests that lateral diffusion of the precursor fragments, either in the gas phase or on the surface, must be relatively unimportant. Instead, as usual, the line width is governed principally by the size of the electron beam and the angular range of the secondary electrons emitted by the surface.

At the earliest stage of growth, discontinuous HfB_2 islands are formed. The size of the HfB_2 islands increases with further deposition, and eventually the islands coalesce to form a continuous line. This behavior indicates that inhomogeneous growth at HfB_2 sites is faster than homogeneous growth along the tip path. The rough morphology of the wires is similar to that seen before.[24] Two mechanisms can account for this rate difference. First, the HfB_2 that is initially deposited may form catalytically active sites for subsequent deposition; thus reactivity is enhanced at initial islands relative to the Si substrate.[30] Second, the initial island sites protrude from the surface so that they are preferential targets for electrons from the tip, thus increasing the deposition rates at these sites in comparison to the surrounding surface.[24]

After STM-EBID, there are bright features in the background around the HfB_2 wires. The density of these features increases with the writing time. Subsequent depassivation confirms that they are silicon dangling bonds. They could be formed by spurious depassivation from the STM tip or by the atomic hydrogen released from the decomposed precursor molecules.

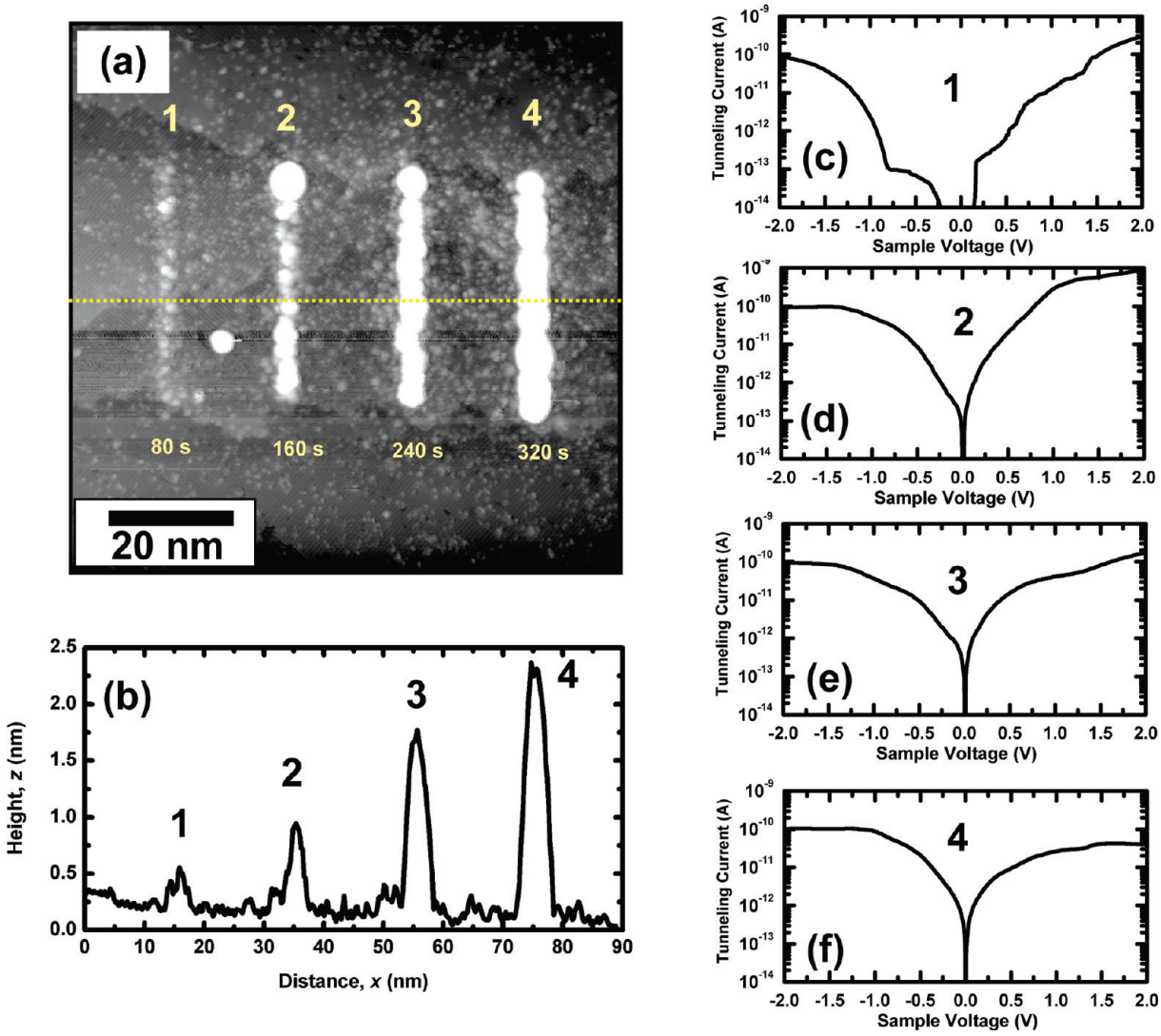

Figure 3. (a) Four HfB_2 nanowires deposited on H-Si(100) surface by STM-EBID. Deposition conditions: sample bias = 5 V, I = 1 nA, Hf-$(BH_4)_4$ background pressure = 2×10^{-9} Torr. (b) STM topographic line contour from (a). (c–f) average I–V tunneling spectra for wires 1–4 shown in (a).

The efficiency of precursor dissociation by the STM electron beam can be estimated from the volume of the HfB_2 nanostructures deposited and the electron dose used. However, so far, all of the writing has been performed at local pressures of $Hf(BH_4)_4$ at or below $\sim 1 \times 10^{-5}$ Torr. Under these conditions, the HfB_2 growth rate increases with the precursor pressure but is insensitive to the writing current or electron dose, which indicates that the writing process is in the transport limited regime. In Figure 4, we plot the number of HfB_2 molecules *versus* writing time for a series of HfB_2 nanowires. These wires were all deposited at 7 V, 0.1 nA, and the local Hf-$(BH_4)_4$ pressure was $\sim 1 \times 10^{-5}$ Torr. The number of molecules was estimated from the apparent volume of the HfB_2 wires and the bulk density of HfB_2. Two growth regimes are clearly seen from the plot. At the initial growth regime, a low growth rate of ~45 molecules/s is observed. We assume that dehydrogena-

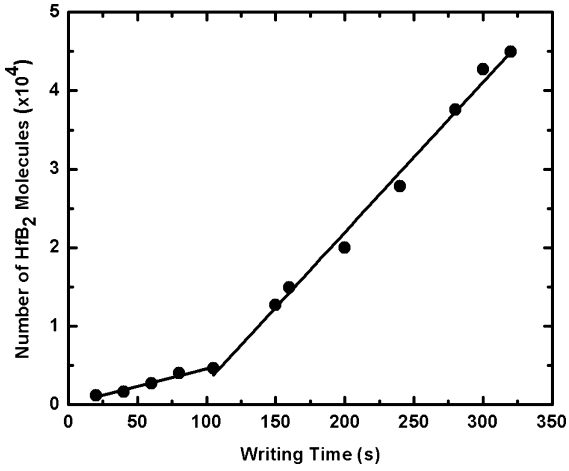

Figure 4. Number of HfB_2 molecules *versus* writing time of a series of HfB_2 nanowires (images not shown) deposited at 7 V and 0.1 nA with a $Hf(BH_4)_4$ pressure of $\sim 1 \times 10^{-5}$ Torr.

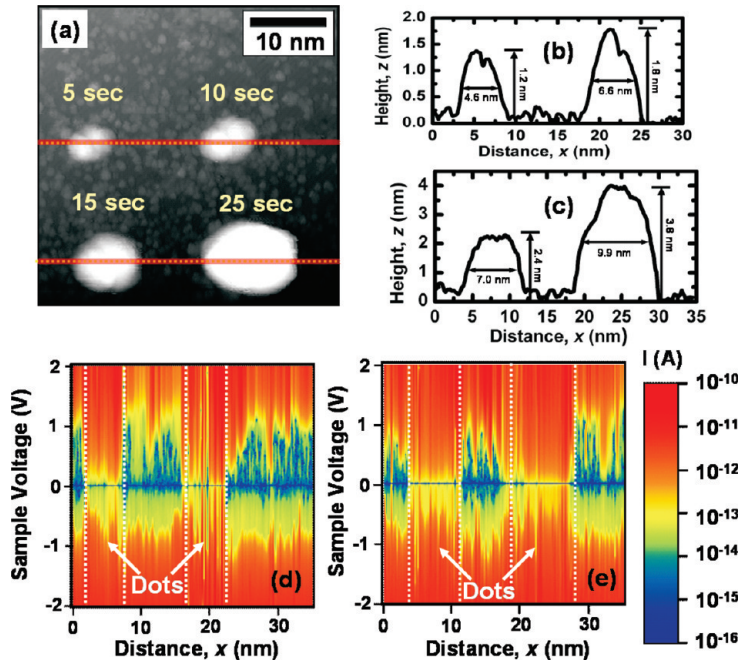

Figure 5. (a) STM topograph of four HfB_2 dots deposited by STM-EBID. Deposition conditions: sample bias = 5 V, I = 1 nA, $Hf(BH_4)_4$ pressure = 4×10^{-6} Torr. The writing time for each dot is 5, 10, 20, and 25 s, respectively. STM line contours are plotted for (b) the top two dots and for (c) the bottom two dots. Log $I-V$ spectra are plotted as a function of position for (d) the top two dots and (e) the bottom two dots. The dotted red lines in (a) denote where the $I-V$ maps were obtained.

tion and HfB_2 nucleation occur in this regime. A higher growth rate of ~191 molecules/s is observed at the second growth regime, in which the subsequent deposition of HfB_2 is on the HfB_2 islands, giving rise to a higher growth rate.

Scanning tunneling spectroscopy (STS) data have also been collected for each HfB_2 nanowire in Figure 3a to confirm metallic behavior. For each wire, 10 $I-V$ spectra were collected at different locations along the wire, mainly on HfB_2 islands. The average $I-V$ spectra are plotted on a semilogarithmic scale in Figure 3c−f. The HfB_2 nanowires are all metallic except line 1, which exhibits a small gap in the $I-V$ spectrum, due to the incomplete coverage of this wire on the substrate. Due to the small size of the HfB_2 nanowires deposited on the surface, their chemical composition cannot be directly analyzed. However, the pure metallic behavior of the nanowires seen by STS suggests that the nanostructures very likely have compositions close to HfB_2, which is the only metallic phase in the Hf−B phase diagram (apart from Hf itself, which is unlikely to be formed under these conditions).

HfB_2 nanodots are deposited by holding the STM tip motionless at one location while dosing with $Hf(BH_4)_4$. Figure 5a shows four HfB_2 nanodots formed by depositions of 5, 10, 20, and 25 s, all with a +5 V sample voltage, a 1 nA tunneling current, and a $Hf(BH_4)_4$ pressure of ~4×10^{-6} Torr. The height profiles of the nanodots are shown in Figure 5b,c.

We clearly see that nanodot height and width both increase with exposure time to the electron beam from the STM tip. The increased widths seen for increased write times are most likely due to the local dissociation rate of precursor exceeding the incorporation rate of HfB_2 into the growing feature. Consequently, molecular fragments can diffuse laterally before being incorporated into the nanodot. Figure 5d,e shows log $I-V$ spectra maps taken along the dotted red lines in Figure 5a, which elucidate local variations in electronic structure of the nanodots and the proximal Si surface. The HfB_2 nanodots show metallic behavior in the $I-V$ maps, whereas the surrounding Si substrate remains semiconducting.

By holding the STM tip at +5 V and employing a 1 nA tunneling current for 1 s, with a $Hf(BH_4)_4$ pressure of ~4×10^{-6} Torr, HfB_2 dots with diameters less than 2.5 nm are deposited, as shown in Figure 6a,b. Figure 6c,d shows the log $I-V$ maps along the dotted red lines in Figure 6a. Despite the small amount of material deposited, the nanodots show pure metallic behavior, indicating that they consist of relatively pure HfB_2.

In summary, metallic HfB_2 nanostructures have been deposited on H-passivated silicon surfaces by local decomposition of $Hf(BH_4)_4$ molecules under a STM tip at room temperature. HfB_2 nanowires with a line width of 4 nm and nanodots as small as 2.5 nm have been successfully deposited. STS data confirm that the nanostructures deposited are purely metallic, indicating that they are essentially pure HfB_2. To our knowledge, this

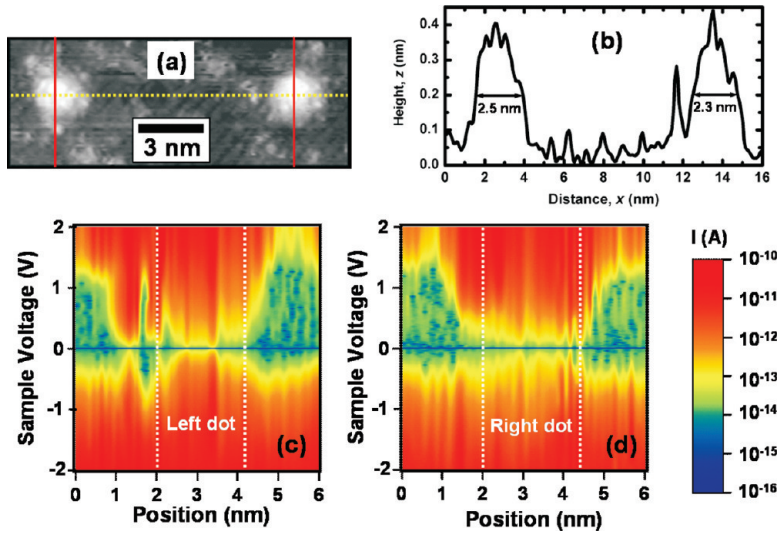

Figure 6. (a) STM topograph of two HfB_2 dots deposited by STM-EBID. Deposition conditions: sample bias = 5 V, I = 1 nA, $Hf(BH_4)_4$ pressure = 4×10^{-6} Torr. The writing time for each dot is 1 s. (b) STM line contour taken along the yellow dotted line in (a). Log $I-V$ spectra plotted as a function of position in (c) for the left dot and (d) the right dot. The solid red lines in (a) denote where the $I-V$ maps were obtained.

is the first demonstration of sub-5 nm metallic nanostructures in an STM-EBID experiment, and it opens new opportunities for making deterministic molecular scale metallic contacts.

EXPERIMENTAL METHODS

Our experiments were performed using a home-built room temperature UHV-STM with a base pressure of less than 7.5×10^{-11} Torr.[32] The $Hf(BH_4)_4$ gas delivery system consists of a $Hf(BH_4)_4$ reservoir, a leak valve, and a stainless steel capillary doser in the UHV chamber. The precursor $Hf(BH_4)_4$ is a solid with a convenient vapor pressure of ~15 Torr at room temperature. The precursor was maintained at 0 °C in a glass vial immersed in an ice−water bath in order to enhance its shelf life. The flow was regulated by the leak valve and delivered to the sample through a 0.4 mm i.d. stainless steel tube pointing directly at the tip−sample junction at a distance of about 1 cm. For this configuration, the local precursor pressure at the tip−sample junction is estimated to be about a factor of 2000 greater than the measured chamber background pressure.[33]

HfB_2 depositions were conducted on B-dopd p-type Si(100)-2 × 1:H substrates with a resistivity of 0.01−0.02 Ω · cm. Electrochemically etched tungsten tips were used for both imaging and metal deposition. Topographic images were acquired in a constant-current mode, current set point was typically 50 pA, and the sample was biased at −2 V. STS data were collected by holding the STM tip at a predefined position within the scan window, disabling the feedback loop, and sweeping the sample voltage from −2 to 2 V while recording the tunneling current.

Acknowledgment. This work was supported by the Defense Advanced Research Project Agency (DARPA) and Space and Naval Warfare Center, San Diego (SPAWARSYSCEN-SD) under Contract N66001-08-C-2040 and by the Office of Naval Research under Grant N00014-06-10120. We also thank the National Science Foundation (CHE07-50422 to G.S.G.) for support.

REFERENCES AND NOTES

1. Shirakashi, J.-I.; Matsumoto, K.; Miura, N.; Konagai, M. Single-Electron Charging Effects in Nb/Nb Oxide-Based Single-Electron Transistors at Room Temperature. *Appl. Phys. Lett.* **1998**, *72*, 1893–1895.
2. Sartale, S. D.; Lin, K.-L.; Chiang, C.-I.; Luo, M.-F.; Kuo, C.-C. Engineering Patterns of Co Nanoclusters on Thin Film Al_2O_3/NiAl(100) Using Scanning Tunneling Microscopy Manipulation Techniques. *Appl. Phys. Lett.* **2006**, *89*, 063113–063118.
3. Vieu, C.; Carcenac, F.; Pépin, A.; Chen, Y.; Mejias, M.; Lebib, A.; Manin-Ferlazzo, L.; Couraud, L.; Launois, H. Electron Beam Lithography: Resolution Limits and Applications. *Appl. Surf. Sci.* **2000**, *164*, 111–117.
4. Lyding, J. W.; Shen, T. C.; Hubacek, J. S.; Tucker, J. R.; Abeln, G. C. Nanoscale Patterning and Oxidation of H-Passivated Si(100)-2 × 1 Surfaces with an Ultrahigh Vacuum Scanning Tunneling Microscope. *Appl. Phys. Lett.* **1994**, *64*, 2010–2012.
5. Walsh, M. A.; Hersam, M. C. Atomic-Scale Templates Patterned by Ultrahigh Vacuum Scanning Tunneling Microscopy on Silicon. *Annu. Rev. Phys. Chem.* **2009**, *60*, 193–216.
6. Adams, D. P.; Mayer, T. M.; Swartzentruber, B. S. Influence of Interfacial Hydrogen on Al Thin Film Nucleation on Si. *J. Appl. Phys.* **1998**, *83*, 4690–4694.
7. Butcher, M. J.; Jones, F. H.; Beton, P. H. Growth and Modification of Ag Islands on Hydrogen Terminated Si(100) Surfaces. *J. Vac. Sci. Technol., B* **2000**, *18*, 13–15.
8. Hashizume, T.; Heike, S.; Lutwyche, M. I.; Watanabe, S.; Nakajima, K.; Nishi, T.; Wada, Y. Interaction of Ga Adsorbates with Dangling Bonds on the Hydrogen Terminated Si(100) Surface. *Jpn. J. Appl. Phys.* **1996**, *35*, L1085.
9. Ilge, B.; Palasantzas, G.; Geerligs, L. J. Submonolayer Growth of Co on H-Passivated Si(100) Surfaces and Nanoscale Metallization with Co on Patterned H-Si(100). *Appl. Surf. Sci.* **1999**, *144−145*, 543–547.
10. Palasantzas, G.; Ilge, B.; De Nijs, J.; Geerligs, L. J. Diffusion, Nucleation and Annealing of Co on the H-Passivated Si(100) Surface. *Surf. Sci.* **1998**, *412−413*, 509–517.
11. Palasantzas, G.; Ilge, B.; De Nijs, J.; Geerligs, L. J. Fabrication of Co/Si Nanowires by Ultrahigh-Vacuum Scanning Tunneling Microscopy on Hydrogen-Passivated Si(100) Surfaces. *J. Appl. Phys.* **1999**, *85*, 1907–1910.
12. Palasantzas, G.; Ilge, B.; Rogge, S.; Geerligs, L. J. Technology for Nanoelectronic Devices Based on Ultra-High Vacuum Scanning Tunneling Microscopy on the Si(100) Surface. *Microelectron. Eng.* **1999**, *46*, 133–136.

13. Sakurai, M.; Thirstrup, C.; Aono, M. Nanoscale Growth of Silver on Prepatterned Hydrogen-Terminated Si(001) Surfaces. *Phys. Rev. B* **2000**, *62*, 16167.
14. Shen, T. C.; Wang, C.; Tucker, J. R. Al Nucleation on Monohydride and Bare Si(001) Surfaces: Atomic Scale Patterning. *Phys. Rev. Lett.* **1997**, *78*, 1271.
15. Adams, D. P.; Mayer, T. M.; Swartzentruber, B. S. Selective Area Growth of Metal Nanostructures. *Appl. Phys. Lett.* **1996**, *68*, 2210–2212.
16. Mitsui, T.; Curtis, R.; Ganz, E. Selective Nanoscale Growth of Titanium on the Si(001) Surface Using an Atomic Hydrogen Resist. *J. Appl. Phys.* **1999**, *86*, 1676–1679.
17. Mitsui, T.; Hill, E.; Curtis, R.; Ganz, E. Adsorption of $TiCl_4$ and Initial Stages of Ti Growth on Si(001). *J. Vac. Sci. Technol., A* **2001**, *19*, 563–567.
18. Mitsui, T.; Hill, E.; Ganz, E. Nanolithography by Selective Chemical Vapor Deposition with an Atomic Hydrogen Resist. *J. Appl. Phys.* **1999**, *85*, 522–524.
19. Shen, T. C.; Wang, C.; Tucker, J. R. The Initial Stage of Nucleation and Growth of Al on H/Si(100)-1 $\times$ 1 by Dimethylaluminum Hydride Vapor Deposition. *Appl. Surf. Sci.* **1999**, *141*, 228–236.
20. Sinniah, K.; Sherman, M. G.; Lewis, L. B.; Weinberg, W. H.; Yates, J. J. T.; Janda, K. C. Hydrogen Desorption from the Monohydride Phase on Si(100). *J. Chem. Phys.* **1990**, *92*, 5700–5711.
21. Botman, A.; Mulders, J. J. L.; Hagen, C. W. Creating Pure Nanostructures from Electron-Beam-Induced Deposition Using Purification Techniques: A Technology Perspective. *Nanotechnology* **2009**, *20*, 372001.
22. Mccord, M. A.; Kern, D. P.; Chang, T. H. P. Direct Deposition of 10-nm Metallic Features with the Scanning Tunneling Microscope. *J. Vac. Sci. Technol., B* **1988**, *6*, 1877–1880.
23. Kent, A. D.; Shaw, T. M.; Von Molnar, S.; Awschalom, D. D. Growth of High Aspect Ratio Nanometer-Scale Magnets with Chemical Vapor Deposition and Scanning Tunneling Microscopy. *Science* **1993**, *262*, 1249–1252.
24. Pai, W. W.; Zhang, J.; Wendelken, J. F.; Warmack, R. J. Magnetic Nanostructures Fabricated by Scanning Tunneling Microscope-Assisted Chemical Vapor Deposition. *J. Vac. Sci. Technol., B* **1997**, *15*, 785–787.
25. Laracuente, A.; Bronikowski, M. J.; Gallagher, A. Chemical Vapor Deposition of Nanometer-Size Aluminum Features on Silicon Surfaces Using an STM Tip. *Appl. Surf. Sci.* **1996**, *107*, 11–17.
26. Rubel, S.; Trochet, M.; Ehrichs, E. E.; Smith, W. F.; De Lozanne, A. L. In *Nanofabrication and Rapid Imaging with a Scanning Tunneling Microscope*, The 1993 International Conference on Tunneling Microscopy; Beijing, China, AVS: Beijing, China, 1994; pp 1894−1897.
27. Saulys, D. S.; Ermakov, A.; Garfunkel, E. L.; Dowben, P. A. Electron-Beam-Induced Patterned Deposition of Allylcyclopentadienyl Palladium Using Scanning Tunneling Microscopy. *J. Appl. Phys.* **1994**, *76*, 7639–7641.
28. Kieffer, R.; Benesovsky, F. *Hartstoffe*; Springer: Berlin, 1963.
29. Jayaraman, S.; Yang, Y.; Kim, D. Y.; Girolami, G. S.; Abelson, J. R. Hafnium Diboride Thin Films by Chemical Vapor Deposition from a Single Source Precursor. *J. Vac. Sci. Technol., A* **2005**, *23*, 1619–1625.
30. Yang, Y.; Jayaraman, S.; Kim, D. Y.; Girolami, G. S.; Abelson, J. R. CVD Growth Kinetics of HfB_2 Thin Films from the Single-Source Precursor $Hf(BH_4)_4$. *Chem. Mater.* **2006**, *18*, 5088–5096.
31. Kumar, N.; Yanguas-Gil, A.; Daly, S. R.; Girolami, G. S.; Abelson, J. R. Remote Plasma Treatment of Si Surfaces: Enhanced Nucleation in Low-Temperature Chemical Vapor Deposition. *Appl. Phys. Lett.* **2009**, *95*, 144107–144103.
32. Lyding, J. W.; Skala, S.; Hubacek, J. S.; Brockenbrough, R.; Gammie, G. Variable-Temperature Scanning Tunneling Microscope. *Rev. Sci. Instrum.* **1988**, *59*, 1897–1902.
33. Campbell, C. T.; Valone, S. M. Design Considerations for Simple Gas Dosers in Surface Science Applications. *J. Vac. Sci. Technol., A* **1985**, *3*, 408–411.